# Mechanistic Theoretical Investigation of Self-Discharge Reactions in a Vanadium Redox Flow Battery

Zhen Jiang,[†] Konstantin Klyukin,[†,§] Kaellen Miller,[†] and Vitaly Alexandrov[*,†,‡]

[†]Department of Chemical and Biomolecular Engineering, University of Nebraska—Lincoln, Lincoln, Nebraska 68588, United States
[‡]Nebraska Center for Materials and Nanoscience, University of Nebraska—Lincoln, Lincoln, Nebraska 68588, United States

S *Supporting Information*

ABSTRACT: Compared to the studies of new electrolyte and electrode chemistries aimed to push the energy and power density of battery systems, investigations of self-discharge reactions contributing to capacity fading are still very limited, especially at the molecular level. Herein, we present a computational study of oxidation−reduction reactions between vanadium ions in solution leading to battery self-discharge due to the crossover of vanadium species through the membrane in all-vanadium redox flow batteries (RFB). By utilizing Car−Parrinello molecular dynamics (CPMD) based metadynamics simulations in combination with the Marcus electron transfer theory, we examine the energetics of condensation reactions between aqueous vanadium ions to form dimers and their subsequent dissociation into vanadium species of different oxidation states after electron transfer has occurred. Our results suggest that multiple self-discharge reaction pathways could be possible under the vanadium RFB operation conditions. The study underscores the complexity of vanadium polymerization reactions in aqueous solutions with coupled electron and proton transfer processes that can lead to the formation of various mixed-valence vanadium polymeric structures.
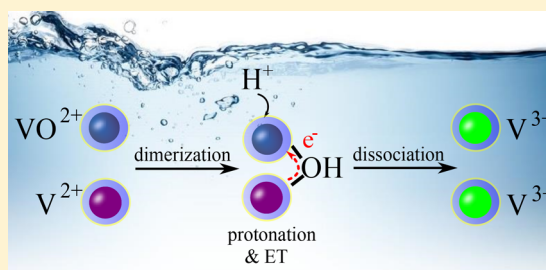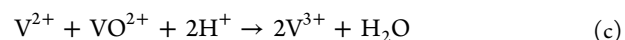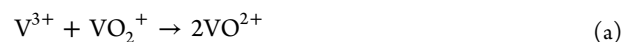
INTRODUCTION

Redox flow batteries (RFBs) have been recently attracting growing attention as a promising large-scale energy storage technology able to store multimegawatt-hours of electrical energy.[1−4] Among various aqueous RFB chemistries proposed to date, all-vanadium RFB is one of the best experimentally studied systems.[5−10] The operation of all-vanadium RFB is based on the electrochemical reactions of the VO^{2+}/VO_2^+ redox couple in the catholyte and the V^{2+}/V^{3+} couple in the anolyte in a sulfuric acid based supporting electrolyte, while each half-cell is separated by an ion-exchange membrane. RFBs store chemical energy in external electrolyte reservoirs, while the redox reactions take place at the electrode surfaces, and thus the energy storage and power generation are decoupled.

Previous experimental investigations have elucidated various aspects of solution and interfacial electrochemistry of aqueous vanadium RFBs that led to significant enhancements of their energy and power density.[6,8,10−13] Recently, a series of atomistic simulations aiming to explore the thermodynamics and kinetics of both electrolyte[11,14−18] and electrode[19,20] vanadium chemistry have also provided complementary molecular insights. For example, both classical and *ab initio* molecular dynamics (AIMD) simulations helped identify solvation structures of vanadium ions in aqueous solutions in the presence of acid electrolyte species including chloride, sulfate, and phosphate.[16−18] AIMD-based enhanced sampling techniques were employed to evaluate thermodynamic stability of aqueous vanadium complexes with electrolyte species,[17,18] pK_a values of the first deprotonation reaction of vanadium

species determining their solubility,[16] as well as free-energy barriers of vanadium redox reactions at the electrode/electrolyte interface.[19,20]

One of the major challenges impeding the long-term performance of RFBs is the loss of battery capacity over time. This is primarily due to the crossover of electrochemically active species such as vanadium ions across the membrane during the battery cycling leading to a range of side reactions. To mitigate capacity fading in RFBs a number of strategies have been proposed including the use of membranes that can minimize vanadium transport between the electrolyte compartments[21−23] or intelligent selection of RFB operating conditions.[24] It was suggested experimentally that a significant contribution to capacity loss may come from internal self-discharge reactions[25,26] associated with crossover of redox-active ions. In the case of all-vanadium RFBs, the following self-discharge reactions can be proposed.

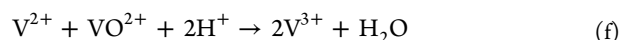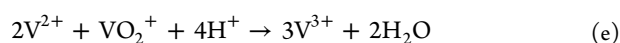In the positive half-cell, V^{2+} and V^{3+} diffused from the negative side may react with VO^{2+} and VO_2^+:

$$V^{3+} + VO_2^+ \rightarrow 2VO^{2+} \tag{a}$$

$$V^{2+} + 2VO_2^+ + 2H^+ \rightarrow 3VO^{2+} + H_2O \tag{b}$$

$$V^{2+} + VO^{2+} + 2H^+ \rightarrow 2V^{3+} + H_2O \tag{c}$$

In the negative half-cell, VO^{2+} and VO_2^+ diffused from the positive side may react with V^{2+} and V^{3+}:

$$V^{3+} + VO_2^+ \rightarrow 2VO^{2+} \tag{d}$$

$$2V^{2+} + VO_2^+ + 4H^+ \rightarrow 3V^{3+} + 2H_2O \tag{e}$$

$$V^{2+} + VO^{2+} + 2H^+ \rightarrow 2V^{3+} + H_2O \tag{f}$$

Note that the reactions a and d are the same and reactions c and f are the same, and they are renumbered as reaction 1 and reaction 3, respectively, whereas reaction b in the positive half-cell and reaction e in the negative half-cell can be combined as the new reaction 2: $V^{2+} + VO_2^+ + 2H^+ \rightarrow VO^{2+} + V^{3+} + H_2O$.

Moreover, it was shown that not only do these self-discharge processes cause capacity losses but also they lead to excessive heating of the vanadium RFBs in stand-by mode.[25,26] This internal heating in turn results in a cascade of other undesired processes such as an increased precipitation of V_2O_5 above 40 °C, which then deposits on the electrodes and blocks the cell channels.[15] The impact of these self-discharge reactions on the vanadium RFB performance was previously evaluated within a thermal model using energy and mass balances to predict the variations in electrolyte temperature and the loss of capacity to help optimize the battery operation conditions.[25,26] To derive the mathematical model, a few assumptions were made including instantaneous character of self-discharge reactions; however, the mechanisms and energetics of these reactions are still unknown. In addition, based on the spectroscopic analysis of the chemical identity of the diffused vanadium cations inside the Nafion membrane,[27] it was hypothesized that self-discharge reactions may be one of the reasons for prevalence of the vanadyl VO^{2+} species accumulated in the membrane.

While it was largely neglected in the past, self-discharge processes occurring during cell operation or rest have recently started attracting more attention across a variety of electric energy storage applications such as supercapacitors,[28] solid-state,[29] and redox-flow[25,26,30] batteries. Understanding their mechanisms is important for the design of low self-discharge systems with minimal energy losses, especially in light of new high-voltage electrode materials. Although there are various mechanisms of self-discharge in batteries such as corrosion, ohmic losses, and faradaic reactions, in this study we focus on condensation reactions between vanadium ions to form dimers followed by internal electron transfer and dissociation into vanadium ions of different oxidation states according to the reactions described above. We note that the formation of a range of vanadium polymeric structures including mixed-valence dimers was shown to occur in various acidic environments;[31,32] however, detailed atomistic information about the mechanisms of self-discharge reactions is still missing. In this study, we investigate such reactions using the density functional theory (DFT) based Car–Parrinello molecular dynamics (CPMD) combined with metadynamics simulations, while the electron transfer processes are examined applying the Marcus electron transfer (ET) theory. It should be also noted that to make the investigation more tractable, we only consider reactions in water environment neglecting the role of multiple factors that may contribute to the self-discharge process such as solution pH, concentrations of vanadium and sulfuric acid in the electrolyte, oxidation of vanadium species in air, and the formation of vanadium clusters more complex than dimers.

■ COMPUTATIONAL DETAILS

Car–Parrinello molecular dynamics (CPMD)[33] simulations were carried out within the plane-wave DFT formalism as implemented in the NWChem code.[34] The electron exchange and correlation were treated employing the Perdew–Burke–Ernzerhof (PBE) functional within the generalized gradient approximation (GGA).[35] The norm-conserving Troullier–Martins pseudopotentials[36] were used for vanadium, and Hamann pseudopotentials[37,38] were used for oxygen and hydrogen. Hydrogen atoms were replaced with deuterium to facilitate numerical integration. The kinetic cutoff energy of 60 Ry was applied to expand the Kohn–Sham electronic wave functions. Γ-point CPMD simulations were performed using a cubic box of length 13 Å with vanadium species and about 72 H_2O molecules to provide the water density of 1 g/cm³ (Figure 1). The Nose–Hoover thermostat[39,40] was employed
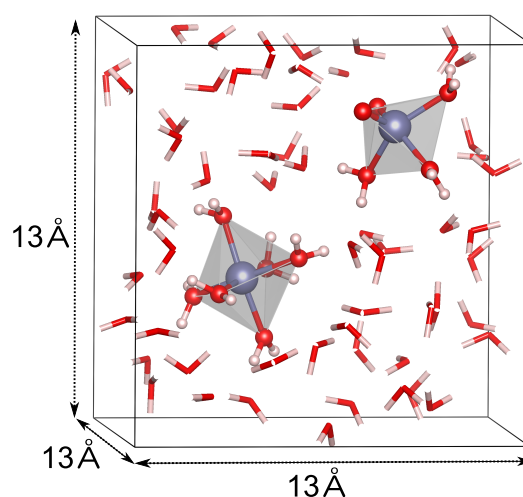
Figure 1. Simulation cell used in CPMD modeling of self-discharge reactions showing V^{3+} and VO_2^+ ions embedded in water solution.

to keep the system temperature at 300 K. All systems were initially pre-equilibrated using a QM/MM potential[41] for 6 ps followed by additional CPMD equilibration for at least 12 ps. A fictitious electronic mass of 600 au and a simulation time step of δt = 5 au (0.121 fs) were employed in all CPMD calculations. CPMD-equilibrated configurations were used for further metadynamics simulations and were saved at time intervals of $10\delta t$. A similar computational scheme was previously exploited by our group to study the properties of isolated vanadium species in aqueous solutions.[16] The effect of sulfate ions commonly present in a VRFB supporting electrolyte was not considered in this study to simplify the analysis of reaction mechanisms. Also, recent computational studies, both classical[18] and *ab initio*[17] molecular dynamics based metadynamics simulations, have shown that the most thermodynamically stable complexes should not have sulfate ions in the first solvation sphere.

To compute the free-energy profiles of condensation and dissociation reactions CPMD-based metadynamics technique was employed. The (width, height) values of the repulsive Gaussian hills (in au) were set to (0.0707, 0.001) for the condensation of monomers and (0.0707, 0.0005) for the dissociation of dimers after internal ET has occurred. Gaussian hills were added to the potential every $100\delta t$ for all reactions considered. The bond distances of $V^{n+}-O^{2-}$ or $V^{n+}-V^{m+}$ were

used as collective variables (CVs) to describe condensation and dissociation reactions. Since the choice of CVs is very important for the correct evaluation of free-energy barriers, we have also performed additional simulations with a set of two CVs, as discussed below. Also, we have estimated the statistical errors associated with evaluation of activation barriers based on the method provided by Laio et al.[42] and also employed in some previous modeling studies.[20,43,44]

To estimate the activation energies of electron transfer for each dimer formed as a result of the condensation reaction, we employed the molecular-orbital formulation of the Marcus ET theory implemented in the NWChem code.[34] This formalism allows one to estimate the activation energy of ET using the thermodynamic driving force of the reaction (the difference between energies of pre- and post-ET complexes in equilibrium, ΔG^0) and the reorganization energy (the energy associated with structural rearrangement and medium polarization due to ET, λ). Strong electronic interaction between the reactant and product states at the crossing point (adiabatic ET) is characterized by a sufficiently large electronic coupling matrix element (V_{AB}) which needs to be taken into account when computing the activation barrier of ET. The details of the approach and its application to a variety of systems can be found elsewhere.[45−49] We note that in this study V_{AB} calculations were carried out within the linearized reaction coordinate approximation[46] as implemented in NWChem. The fragment molecular orbital method in which a molecular cluster is divided into multiple fragments was employed to overcome the problem of large-scale diagonalization and multiple electron integrals in conventional electronic structure calculations.[50] The dimer structures were optimized within the DFT method using the hybrid B3LYP functional along with 6-31G** basis set for vanadium and 6-311G** basis set for oxygen and hydrogen atoms. Also, the Mulliken population analysis was employed to estimate atomic charges and magnetic moments to help interpret the formal oxidation states of vanadium ions (see Supporting Information).

■ RESULTS AND DISCUSSION

Hydration structures of isolated vanadium ions were previously identified by means of both static DFT[51] and AIMD[14,16] simulations. On the basis of room-temperature CPMD calculations,[16] the most stable forms of V^{2+}, V^{3+}, VO^{2+}, and VO_2^+ ions in aqueous solution are $V(H_2O)_6^{2+}$, $V(H_2O)_6^{3+}$, $VO(H_2O)_5^{2+}$, and $VO_2(H_2O)_3^+$, respectively. Our CPMD simulations also reveal spontaneous deprotonation and protonation of $VO_2^+(H_2O)_3$ leading to the formation of vanadic acid $VO(OH)_3$ species after 40 ps at room temperature. This is consistent with another CPMD study suggesting that $VO(OH)_3$ may be the preferred V^{5+} state in an acidic aqueous environment at 500 K.[14] Experimentally, H_3VO_4 species in solution were also identified at high temperature (>335 K) by NMR spectroscopy.[15] Therefore, in our modeling of self-discharge reactions involving V^{5+} we examine both $VO_2^+(H_2O)_3$ and $VO(OH)_3$ species.

It is believed that polymerization reactions between aqueous vanadium species that eventually lead to the formation of vanadium oxide precipitates proceed through condensation reactions.[15,32,52,53] The first step of this process is deprotonation of an H_2O molecule from the first coordination sphere of a vanadium ion, and thus the propensity for polymerization can be related to the pK_a values. According to previous *ab initio* simulations,[14,16] $VO_2^+(H_2O)_3$ is characterized by the lowest

activation barrier for the first deprotonation reaction among all the four vanadium ions and a pK_a value of about 3.06, in agreement with experimental data.[54] This turns out to agree well with our estimates of free-energy barriers of dimerization involving VO_2^+, as alluded to the discussion below. The next reaction step is the formation of a dimer between two metal centers via O and/or OH bridging groups,[55−57] which may also include the removal of H_2Os from the first coordination sphere. It is then followed by ET (spontaneous or activated) and dissociation of the post-ET dimer into two product monomers. In the following, we analyze vanadium self-discharge reactions by estimating the energetics of all the steps using the combination of CPMD-based metadynamics and molecular-cluster ET calculations.

Reaction 1.

$$V^{3+} + VO_2^+ \rightarrow 2VO^{2+} \qquad (1)$$

Figure 2 shows the details of CPMD metadynamics simulations employed to model dimerization reaction between
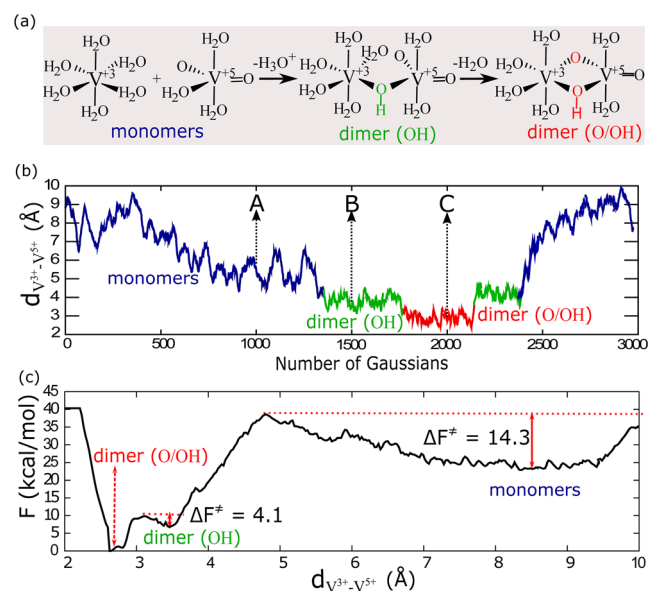
Figure 2. Dimerization reaction between $V^{3+}(H_2O)_6$ and $VO_2^+(H_2O)_3$ in aqueous solution at 300 K as determined by CPMD metadynamics: (a) reaction mechanism, (b) evolution of the collective variable (the bond distance between V^{3+} and V^{5+}) as a function of the added Gaussians, and (c) free energy profile of the overall condensation reaction. Atomic structures corresponding to points A, B, and C along the reaction pathway in part b are shown in Figure 3.

$V^{3+}(H_2O)_6$ and $VO_2^+(H_2O)_3$, while Figure 3 depicts the atomic structures associated with the major reaction steps of the process. It is found that the reaction starts with two monomers forming a dimer bridged by a single OH group. This involves hydrolysis of a first-shell H_2O molecule from $VO_2^+(H_2O)_3$ and departure of H_2O from the first shell of $V(H_2O)_6^{3+}$ (see the transition from structure A to B in Figure 3). Next, the formation of the second O bridge between the two vanadium ions occurs accompanied by the escape of one H_2O molecule from the first water shell of V^{3+}. The corresponding evolution of CV ($V^{3+}-V^{5+}$ distance) as a function of the number of Gaussians and the reconstructed free-energy profile associated with the process are shown in Figure 2, parts b and c, respectively. The rate-determining step

3978
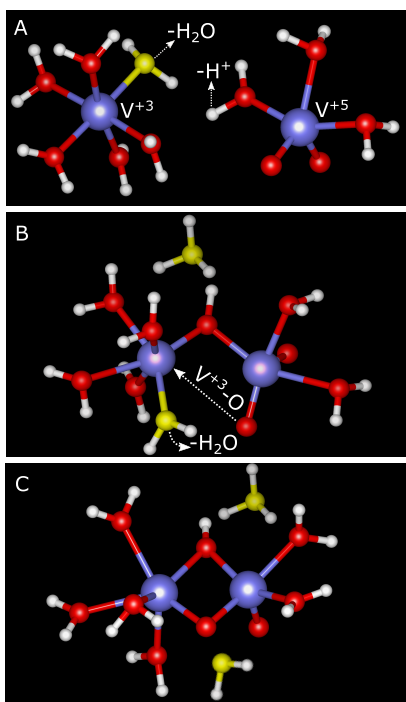
Figure 3. Atomic-structure snapshots from the CPMD metadynamics trajectory of dimerization reaction between $V^{3+}(H_2O)_6$ and $VO_2^+(H_2O)_3$ corresponding to points A, B, and C in Figure 2b chosen after the addition of 1000, 1500, and 2000 Gaussians, respectively. Water molecules beyond the first shells of the V ions are removed for clarity.

is found to be the formation of the first OH bridge with an energy cost of about ~14 kcal/mol, whereas the formation of an additional O bridge may be expected to occur spontaneously at room temperature due to the low activation barrier of around ~4 kcal/mol with the estimated error discussed below.

The energetics of ET process to produce the $V^{4+}-V^{4+}$ dimer from the newly formed $V^{3+}-V^{5+}$ complex that can subsequently dissociate into two V^{4+} monomers to complete the self-discharge reaction was then estimated within the Marcus ET theory. The calculated ET barrier (ΔG^*) of about 23 kcal/mol between complexes **1A** and **1B** (see Figure 4) with the electronic coupling constant (V_{AB}) of only 0.8 kcal/mol suggests ET to be the rate-limiting step toward the formation of VO^{2+}. The protonation of any O or OH group in complex **1A** is found to be unfavorable based on our CPMD simulations involving solution H_3O^+ species. Figure 5 shows the V−O bond distances of the corresponding pre- (**1A**) and post-ET (**1B**) complexes revealing the involvement of the O bridge into ET process. Unlike the transformation from **1A** to **1B** for the complex involving only a single OH bridge (see Figure 2a), it was impossible to stabilize the post-ET $V^{4+}-V^{4+}$ structure based on additional ET calculations. When complex **1B** is embedded into aqueous solution for equilibration, it gains one more H_2O to yield complex **1C**. Then, the free-energy barrier of **1C** dissociation into two V^{4+} species is estimated by metadynamics simulations at 18.5 kcal/mol.

Since V^{5+} can be present in aqueous electrolyte in the form of vanadic acid,[14,15,58] we also examine its interaction with V^{3+}. Figure 6 shows the reaction pathway and associated activation barriers for each reaction step identified by metadynamics and ET calculations. The first step is the dimerization reaction
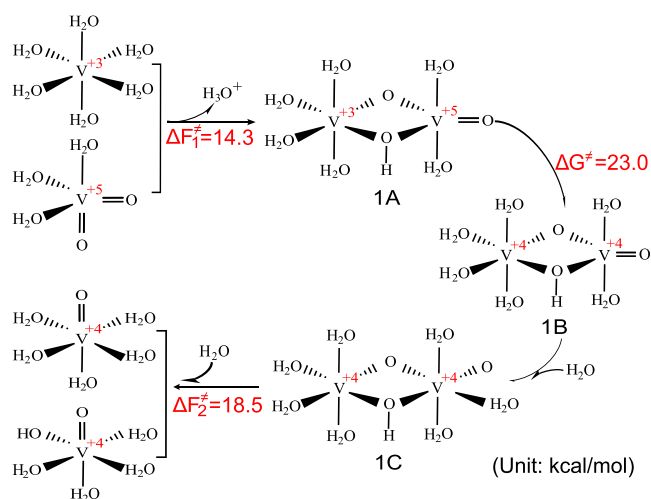
Figure 4. Reaction mechanism and estimated activation barriers (in kcal/mol) for the ionic and electronic reaction steps associated with the self-discharge reaction 1.
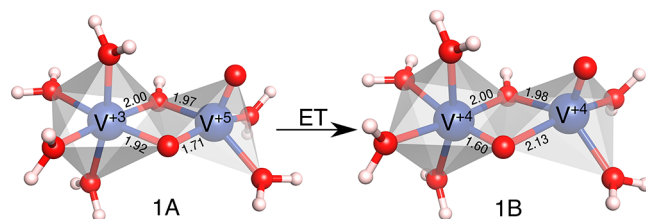
Figure 5. Vanadium dimers used to estimate ET barriers along with the V−O bond lengths for pre- and post-ET complexes in reaction 1 (Figure 4).
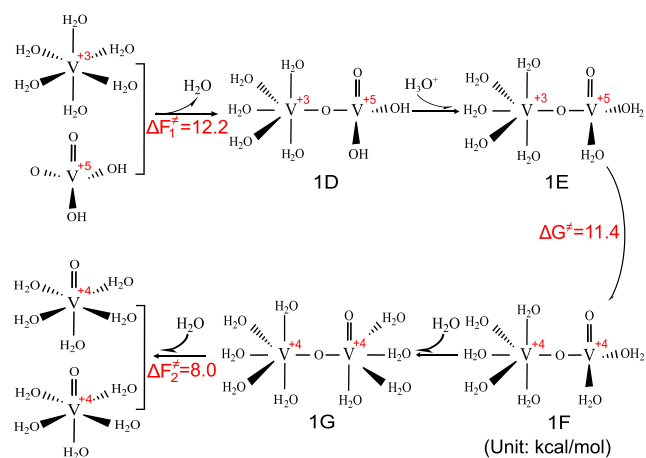
Figure 6. Reaction mechanism and estimated activation barriers (in kcal/mol) for the ionic and electronic reaction steps associated with the self-discharge reaction using vanadic acid as a V^{5+} source.

between $V^{3+}(H_2O)_6$ and $H_2VO_4^-$, where $H_2VO_4^-$ is spontaneously formed upon deprotonation of H_3VO_4. We find that this condensation reaction has a 12.2 kcal/mol activation barrier to produce complex **1D**. Subsequent equilibration of **1D** in acidic solution involving H_3O^+'s reveals that complex **1D** gets spontaneously protonated to produce **1E**. The electron hopping in **1E** to yield post-ET complex **1F** is computed to have an energy barrier of about 11.4 kcal/mol. Figure 7 shows the V−O interatomic distances for both pre-
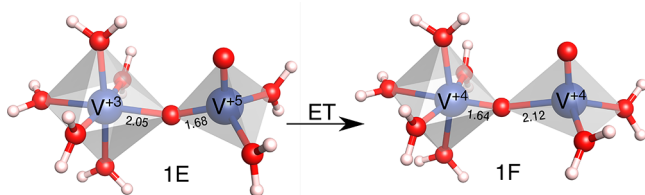
Figure 7. Vanadium dimers used to estimate ET barriers along with the V−O bond lengths for pre- and post-ET complexes in reaction 1 (Figure 6).

and post-ET complexes. The lower ET barrier in this case as compared to the reaction 1A → 1B can be related to a lower reorganization energy necessary to adjust the geometry with only one O bridge situated close to the line connecting two vanadium centers. According to CPMD equilibration, when embedded in solution complex **1F** spontaneously gains one more H_2O in the first hydration shell to complete 6-fold coordination of both V^{4+} ions in the dimer structure (complex **1G**). Then, approximately 8 kcal/mol activation barrier is required to dissociate the formed dimer **1G** into two $VO^{2+}(H_2O)_5$ complexes.

Reaction 2.

$$V^{3+} + VO_2^+ + 2H^+ \rightarrow VO^{2+} + V^{3+} + H_2O \qquad (2)$$
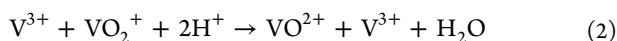
We next analyze the mechanism and kinetics of self-discharge reaction between V^{2+} and V^{5+} considering both $VO_2^+(H_2O)_3$ and vanadic acid complexes, similarly to the V^{3+} case discussed above. The main distinctive feature of this self-discharge reaction pathway is that the ET step is observed to be spontaneous and coupled to protonation, either internal (Figure 8) or external (Figure 9). Figure 8 shows that V^{2+}
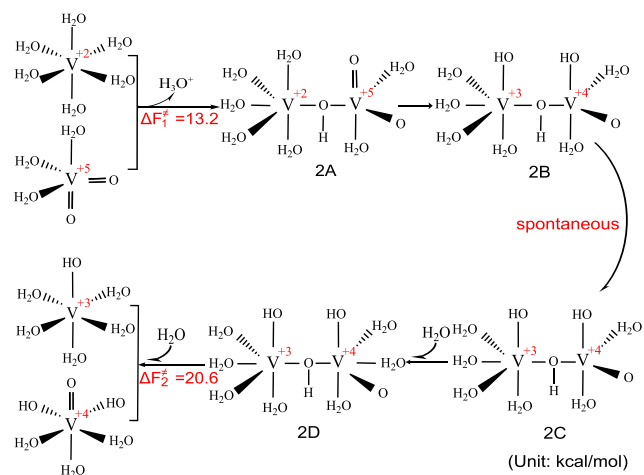
Figure 8. Reaction mechanism and estimated activation barriers (in kcal/mol) for the ionic and electronic reaction steps associated with the self-discharge reaction 2.

and VO_2^+ first form a dimer via an OH bridge as a result of the first deprotonation reaction of $VO_2^+(H_2O)_3$, in agreement with a lower pK_a value of VO_2^+.[14,16,54] Once dimer **2A** is formed a proton from H_2O of the V^{2+} center is transferred spontaneously to the neighboring O atom of V^{5+} (complex **2B**) accompanied by spontaneous ET to yield complex **2C**. Further equilibration of **2C** results in the formation of a more stable complex **2D** by adsorbing one more H_2O from solution.

Figure 9. Reaction mechanism and estimated activation barriers (in kcal/mol) for the ionic and electronic reaction steps associated with the self-discharge reaction 2, using vanadic acid as a V^{5+} source.
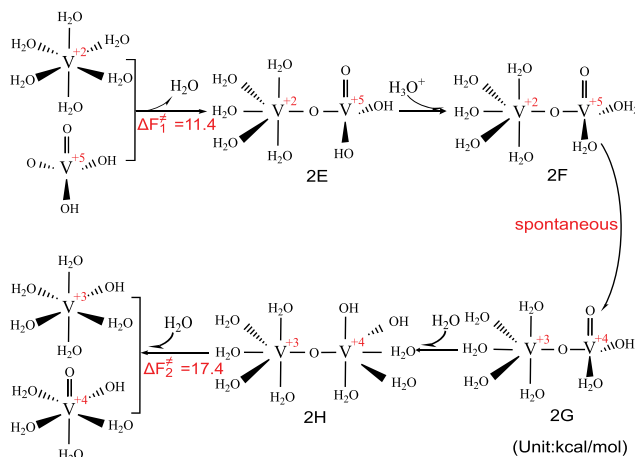
The activation barrier for this whole process is estimated at 13.2 kcal/mol from metadynamics simulations. The spontaneous nature of ET and its coupling to internal proton transfer is further confirmed by gas-phase DFT optimization using cluster **2A**. The final dissociation step to produce V^{3+} and V^{4+} monomers from **2D** is estimated to have an activation energy of about 20.6 kcal/mol. The reaction between V^{2+} and vanadic acid complex is found to follow the same reaction steps including spontaneous ET triggered by external protonation from solution H_3O^+ rather than internal protonation (Figure 9). Energetically, however, the reaction with vanadic acid species features slightly smaller activation barriers for both dimerization (11.4 kcal/mol) and dissociation (17.4 kcal/mol).

Reaction 3.

$$V^{2+} + VO^{2+} + 2H^+ \rightarrow 2V^{3+} + H_2O \qquad (3)$$
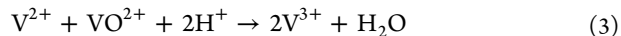
Figure 10 summarizes the self-discharge reaction mechanism involving V^{2+} and VO^{2+} to produce two V^{3+} species. Overall, we find that this reaction is characterized by the lowest-energy reaction steps among all the analyzed self-discharge reactions.
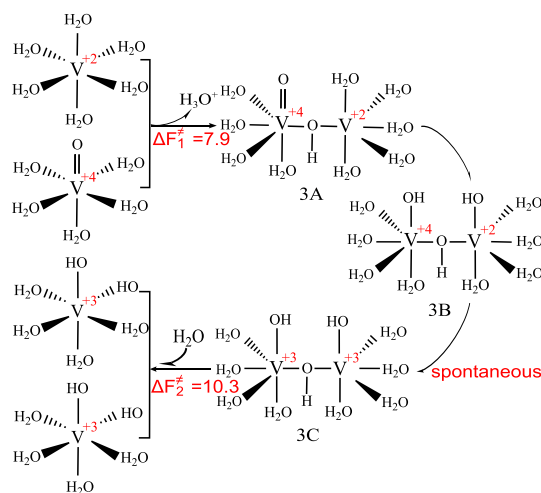
Figure 10. Reaction mechanism and estimated activation barriers (in kcal/mol) for the ionic and electronic reaction steps associated with the self-discharge reaction 3.

Table 1. Summary of the Free-Energy Barriers Estimated from Metadynamics along with Associated Errors for the Condensation and Dissociation Reactions (in kcal/mol)[a]

	reaction 1	reaction 1*	reaction 2	reaction 2*	reaction 3
Dimerization ($\Delta F_1^{\neq}$)	14.3 ± 1.9	12.2 ± 1.8	13.2 ± 1.9	11.4 ± 1.5	7.9 ± 2.3
Dissociation ($\Delta F_2^{\neq}$)	18.5 ± 1.2	8.0 ± 1.5	20.6 ± 1.4	17.4 ± 1.2	10.3 ± 1.4

[a]An asterisk (∗) denotes the reactions involving V^{5+} in the form of vanadic acid.

Specifically, the first dimerization step accounts for an activation energy of 7.9 kcal/mol, while the last dissociation step features a free-energy barrier of around 10 kcal/mol. The ET step turns out to be spontaneous and coupled to internal protonation to allow **3A → 3B → 3C** transformations. The electronic configurations and spontaneous nature of ET are also confirmed by static DFT calculations carried out on the dimer molecules. Therefore, the obtained results suggest that reaction 3 should be energetically favorable self-discharge pathway in vanadium RFBs consuming V^{2+} and VO^{2+} to produce V^{3+} species.

Error Evaluation. In this section, we estimate the statistical errors associated with evaluation of free-energy barriers from *ab initio* metadynamics for the reactions under study. The details of the method used to calculate these errors can be found elsewhere.[20,42,59] The obtained errors are listed along with the corresponding activation barriers in Table 1. It is seen that the errors generally do not exceed 2 kcal/mol ($\sim 3k_BT$), which is consistent with other studies where similar computational schemes were employed.[43,44]

To provide insight into the effect of the chosen CV in metadynamics simulations on the estimated activation barriers, we also compare free-energy barriers obtained using one and two CVs on the example of V^{2+}/VO^{2+} dimerization reaction. The first case corresponds to a single CV which is the bond distance between V^{2+} and V^{4+}. The activation barrier for this reaction, as discussed before, is found to be 7.9 kcal/mol as seen from the free-energy profile shown in Figure 11. The
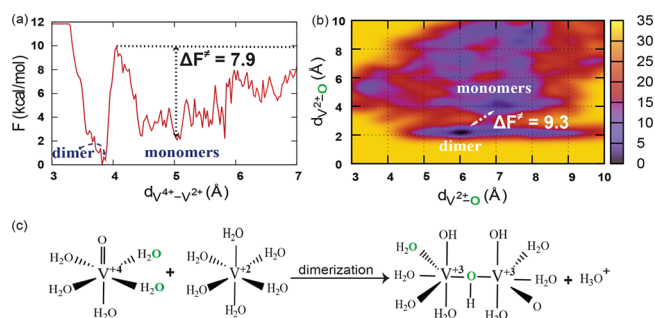
Figure 11. 1D (a) and 2D (b) free-energy maps corresponding to metadynamics simulations with one and two CVs, respectively, for the dimerization reaction between $V^{2+}(H_2O)_6$ and $VO^{2+}(H_2O)_5$ (c). CV in part a is the $V^{2+}-V^{4+}$ bond distance and CVs in part b are the two $V^{2+}-O$ bond distances, where O is from two H_2Os in $VO^{2+}(H_2O)_5$.

same reaction is also modeled using a two-dimensional CV space, where dimerization of two vanadium monomers is defined by the distance between the V^{2+} center and two oxygen atoms from the water molecules in the first hydration shell of V^{4+}. For this set of CVs the activation barrier is determined to be slightly higher than for a single CV being around 9.3 kcal/mol (see in Figure 11b). The reaction with both sets of CVs resulted in the same dimer complex with one OH bridge between the two vanadium metal centers, while the activation

energy estimated with one CV is comparable to the one obtained using two CVs given the error bar.

■ CONCLUSIONS

In this study, we employed CPMD-based metadynamics simulations in conjunction with the Marcus electron transfer theory to investigate vanadium dimerization and self-discharge reactions that could occur due to the crossover of vanadium species between the two half-cell compartments in all-vanadium RFBs. The atomistic mechanisms and related activation barriers for both ionic and electron transfer steps are determined for various reaction pathways. The reactions are found to proceed through a sequence of steps comprised of the hydrolysis and condensation reaction between two aqueous vanadium monomers, electron transfer process (spontaneous or activated, coupled to proton transfer or not), and subsequent dissociation of the dimers into two monomers with vanadium cations in different oxidation states. We find that various self-discharge reaction pathways can be possible under operation conditions of the all-vanadium RFBs leading to preferential consumption/production of vanadium ions. For example, we find that self-discharge should contribute to the formation of the vanadyl VO^{2+} ions which were the only experimentally observable vanadium species inside the Nafion membrane. However, the relative contribution of each specific self-discharge reaction should depend on multiple factors not considered in the present study such as oxidation of vanadium ions in air, solution pH, and the concentration of electrolyte species. On the basis of the obtained results, a number of mixed-valence vanadium dimers are expected to form, which may also serve as precursors for the formation of vanadium polymeric structures with different redox properties than the parent vanadium ions. In general, the electrolyte chemistries that inhibit hydrolysis of aqueous vanadium species should also hinder vanadium polymerization and self-discharge reactions and thus decrease the battery capacity losses.

■ ASSOCIATED CONTENT

ⓈSupporting Information
The Supporting Information is available free of charge on the ACS Publications website at DOI: 10.1021/acs.jpcb.8b10980.

Mulliken population analysis for the dimers and data for the dimerization and dissociation reactions from Car−Parrinello molecular dynamics based metadynamics simulations (evolution of the collective variables versus the number of Gaussians and reconstructed free energy profiles) (PDF)

■ AUTHOR INFORMATION

Corresponding Author
*(V.A.) E-mail: valexandrov2@unl.edu. Telephone: +1 402 4725323.
ORCID ⓘ
Zhen Jiang: 0000-0002-1175-5658

Konstantin Klyukin: 0000-0001-8325-8725
Vitaly Alexandrov: 0000-0003-2063-6914

Present Address

§Department of Materials Science and Engineering, Massachusetts Institute of Technology, 77 Massachusetts Avenue, Cambridge, MA, 02139, USA

Notes

The authors declare no competing financial interest.

REFERENCES

(1) Weber, A. Z.; Mench, M. M.; Meyers, J. P.; Ross, P. N.; Gostick, J. T.; Liu, Q. Redox flow batteries: a review. *J. Appl. Electrochem.* **2011**, *41*, 1137.

(2) Alotto, P.; Guarnieri, M.; Moro, F. Redox flow batteries for the storage of renewable energy: A review. *Renewable Sustainable Energy Rev.* **2014**, *29*, 325−335.

(3) Soloveichik, G. L. Flow batteries: current status and trends. *Chem. Rev.* **2015**, *115*, 11533−11558.

(4) Skyllas-Kazacos, M.; Rychcik, M.; Robins, R. G.; Fane, A.; Green, M. New all-vanadium redox flow cell. *J. Electrochem. Soc.* **1986**, *133*, 1057.

(5) Kear, G.; Shah, A. A.; Walsh, F. C. Development of the all-vanadium redox flow battery for energy storage: a review of technological, financial and policy aspects. *Int. J. Energy Res.* **2012**, *36*, 1105−1120.

(6) Parasuraman, A.; Lim, T. M.; Menictas, C.; Skyllas-Kazacos, M. Review of material research and development for vanadium redox flow battery applications. *Electrochim. Acta* **2013**, *101*, 27−40.

(7) Huang, Q.; Wang, Q. Next-Generation, High-Energy-Density Redox Flow Batteries. *ChemPlusChem* **2015**, *80*, 312−322.

(8) Ding, C.; Zhang, H.; Li, X.; Liu, T.; Xing, F. Vanadium flow battery for energy storage: prospects and challenges. *J. Phys. Chem. Lett.* **2013**, *4*, 1281−1294.

(9) Leung, P.; Li, X.; Ponce De León, C.; Berlouis, L.; Low, C. J.; Walsh, F. C. Progress in redox flow batteries, remaining challenges and their applications in energy storage. *RSC Adv.* **2012**, *2*, 10125−10156.

(10) Kim, K. J.; Park, M.-S.; Kim, Y.-J.; Kim, J. H.; Dou, S. X.; Skyllas-Kazacos, M. A Technology Review of Electrodes and Reaction Mechanisms in Vanadium Redox Flow Batteries. *J. Mater. Chem. A* **2015**, *3*, 16913−16933.

(11) Vijayakumar, M.; Nie, Z.; Walter, E.; Hu, J.; Liu, J.; Sprenkle, V.; Wang, W. Understanding Aqueous Electrolyte Stability through Combined Computational and Magnetic Resonance Spectroscopy: A Case Study on Vanadium Redox Flow Battery Electrolytes. *ChemPlusChem* **2015**, *80*, 428−437.

(12) Noack, J.; Roznyatovskaya, N.; Herr, T.; Fischer, P. The Chemistry of Redox-Flow Batteries. *Angew. Chem., Int. Ed.* **2015**, *54*, 9776−9809.

(13) Skyllas-Kazacos, M.; Cao, L.; Kazacos, M.; Kausar, N.; Mousa, A. Vanadium Electrolyte Studies for the Vanadium Redox Battery: a Review. *ChemSusChem* **2016**, *9*, 1521−1543.

(14) Sadoc, A.; Messaoudi, S.; Furet, E.; Gautier, R.; Le Fur, E.; Le Polles, L.; Pivan, J.-Y. Structure and Stability of VO_2^+ in Aqueous Solution: A Car- Parrinello and Static ab Initio Study. *Inorg. Chem.* **2007**, *46*, 4835−4843.

(15) Vijayakumar, M.; Li, L.; Graff, G.; Liu, J.; Zhang, H.; Yang, Z.; Hu, J. Z. Towards understanding the poor thermal stability of V^{5+} electrolyte solution in vanadium redox flow batteries. *J. Power Sources* **2011**, *196*, 3669−3672.

(16) Jiang, Z.; Klyukin, K.; Alexandrov, V. Structure, hydrolysis, and diffusion of aqueous vanadium ions from Car-Parrinello molecular dynamics. *J. Chem. Phys.* **2016**, *145*, 114303.

(17) Bon, M.; Laino, T.; Curioni, A.; Parrinello, M. Characterization of Vanadium Species in Mixed Chloride−Sulfate Solutions: An Ab Initio Metadynamics Study. *J. Phys. Chem. C* **2016**, *120*, 10791−10798.

(18) Gupta, S.; Lim, T. M.; Mushrif, S. H. Insights into the solvation of vanadium ions in the vanadium redox flow battery electrolyte using molecular dynamics and metadynamics. *Electrochim. Acta* **2018**, *270*, 471−479.

(19) Jiang, Z.; Klyukin, K.; Alexandrov, V. First-principles study of adsorption−desorption kinetics of aqueous V^{2+}/V^{3+} redox species on graphite in a vanadium redox flow battery. *Phys. Chem. Chem. Phys.* **2017**, *19*, 14897−14901.

(20) Jiang, Z.; Klyukin, K.; Alexandrov, V. Ab Initio Metadynamics Study of VO_2^+/VO^{2+} Redox Reaction Mechanism at the Graphite Edge-Water Interface. *ACS Appl. Mater. Interfaces* **2018**, *10*, 20621−20626.

(21) Schulte, D.; Drillkens, J.; Schulte, B.; Sauer, D. U. Nafion Hybrid Membranes for Use in Redox Flow Batteries. *J. Electrochem. Soc.* **2010**, *157*, A989−A992.

(22) Chen, D.; Hickner, M. A.; Agar, E.; Kumbur, E. C. Optimized Anion Exchange Membranes for Vanadium Redox Flow Batteries. *ACS Appl. Mater. Interfaces* **2013**, *5*, 7559−7566.

(23) Nibel, O.; Bon, M.; Agiorgousis, M. L.; Laino, T.; Gubler, L.; Schmidt, T. J. Unraveling the Interaction Mechanism between Amidoxime Groups and Vanadium Ions at Various pH Conditions. *J. Phys. Chem. C* **2017**, *121*, 6436−6445.

(24) Agar, E.; Benjamin, A.; Dennison, C.; Chen, D.; Hickner, M.; Kumbur, E. Reducing capacity fade in vanadium redox flow batteries by altering charging and discharging currents. *J. Power Sources* **2014**, *246*, 767−774.

(25) Tang, A.; Bao, J.; Skyllas-Kazacos, M. Dynamic modelling of the effects of ion diffusion and side reactions on the capacity loss for vanadium redox flow battery. *J. Power Sources* **2011**, *196*, 10737−10747.

(26) Tang, A.; Bao, J.; Skyllas-Kazacos, M. Thermal modelling of battery configuration and self-discharge reactions in vanadium redox flow battery. *J. Power Sources* **2012**, *216*, 489−501.

(27) Vijayakumar, M.; Bhuvaneswari, M.; Nachimuthu, P.; Schwenzer, B.; Kim, S.; Yang, Z.; Liu, J.; Graff, G. L.; Thevuthasan, S.; Hu, J. Spectroscopic investigations of the fouling process on Nafion membranes in vanadium redox flow batteries. *J. Membr. Sci.* **2011**, *366*, 325−334.

(28) Xia, M.; Nie, J.; Zhang, Z.; Lu, X.; Wang, Z. L. Suppressing self-discharge of supercapacitors via electrorheological effect of liquid crystals. *Nano Energy* **2018**, *47*, 43−50.

(29) Chung, S.-H.; Han, P.; Manthiram, A. Quantitative analysis of electrochemical and electrode stability with low self-discharge lithium-sulfur batteries. *ACS Appl. Mater. Interfaces* **2017**, *9*, 20318−20323.

(30) Murali, A.; Nirmalchandar, A.; Krishnamoorthy, S.; Hoober-Burkhardt, L.; Yang, B.; Soloveichik, G.; Prakash, G. S.; Narayanan, S. Understanding and Mitigating Capacity Fade in Aqueous Organic Redox Flow Batteries. *J. Electrochem. Soc.* **2018**, *165*, A1193−A1203.

(31) Madic, C.; Begun, G. M.; Hahn, R. L.; Launay, J. P.; Thiessen, W. E. Dimerization of aquadioxovanadium(V) ion in concetated perchloric and sulfuric acid media. *Inorg. Chem.* **1984**, *23*, 469−476.

(32) Roznyatovskaya, N. V.; Roznyatovsky, V. A.; Höhne, C.-C.; Fühl, M.; Gerber, T.; Küttinger, M.; Noack, J.; Fischer, P.; Pinkwart, K.; Tübke, J. The role of phosphate additive in stabilization of sulphuric-acid-based vanadium (V) electrolyte for all-vanadium redox-flow batteries. *J. Power Sources* **2017**, *363*, 234−243.

(33) Car, R.; Parrinello, M. Unified approach for molecular dynamics and density-functional theory. *Phys. Rev. Lett.* **1985**, *55*, 2471.

(34) Valiev, M.; Bylaska, E. J.; Govind, N.; Kowalski, K.; Straatsma, T. P.; Van Dam, H. J.; Wang, D.; Nieplocha, J.; Apra, E.; Windus, T. L.; et al. NWChem: a comprehensive and scalable open-source solution for large scale molecular simulations. *Comput. Phys. Commun.* **2010**, *181*, 1477−1489.

(35) Perdew, J. P.; Burke, K.; Ernzerhof, M. Generalized gradient approximation made simple. *Phys. Rev. Lett.* **1996**, *77*, 3865.

(36) Troullier, N.; Martins, J. L. Efficient pseudopotentials for plane-wave calculations. *Phys. Rev. B: Condens. Matter Mater. Phys.* **1991**, *43*, 1993.

(37) Hamann, D.; Schlüter, M.; Chiang, C. Norm-conserving pseudopotentials. *Phys. Rev. Lett.* **1979**, *43*, 1494.

(38) Hamann, D. Generalized norm-conserving pseudopotentials. *Phys. Rev. B: Condens. Matter Mater. Phys.* **1989**, *40*, 2980.

(39) Nosé, S. A molecular dynamics method for simulations in the canonical ensemble. *Mol. Phys.* **1984**, *52*, 255−268.

(40) Hoover, W. G. Canonical dynamics: equilibrium phase-space distributions. *Phys. Rev. A: At., Mol., Opt. Phys.* **1985**, *31*, 1695.

(41) Cauët, E.; Bogatko, S.; Weare, J. H.; Fulton, J. L.; Schenter, G. K.; Bylaska, E. J. Structure and dynamics of the hydration shells of the Zn^{2+} ion from ab initio molecular dynamics and combined ab initio and classical molecular dynamics simulations. *J. Chem. Phys.* **2010**, *132*, 194502.

(42) Laio, A.; Gervasio, F. L. Metadynamics: a Method to Simulate Rare Events and Reconstruct the Free Energy in Biophysics, Chemistry and Material Science. *Rep. Prog. Phys.* **2008**, *71*, 126601.

(43) Stirling, A.; Pápai, I. H_2CO_3 Forms via HCO_3^- in Water. *J. Phys. Chem. B* **2010**, *114*, 16854−16859.

(44) Stirling, A. HCO_3^--Formation from CO_2 at High pH: Ab Initio Molecular Dynamics Study. *J. Phys. Chem. B* **2011**, *115*, 14683−14687.

(45) Marcus, R. A.; Sutin, N. Electron transfers in chemistry and biology. *Biochim. Biophys. Acta, Rev. Bioenerg.* **1985**, *811*, 265−322.

(46) Farazdel, A.; Dupuis, M.; Clementi, E.; Aviram, A. Electric-field induced intramolecular electron transfer in spiro. pi.-electron systems and their suitability as molecular electronic devices. A theoretical study. *J. Am. Chem. Soc.* **1990**, *112*, 4206−4214.

(47) Marcus, R. A. Electron transfer reactions in chemistry - theory and experiment. *Rev. Mod. Phys.* **1993**, *65*, 599−610.

(48) Alexandrov, V.; Neumann, A.; Scherer, M. M.; Rosso, K. M. Electron exchange and conduction in nontronite from first-principles. *J. Phys. Chem. C* **2013**, *117*, 2032−2040.

(49) Nielsen, M. T.; Moltved, K. A.; Kepp, K. P. Electron Transfer of Hydrated Transition-Metal Ions and the Electronic State of Co^{3+} (aq). *Inorg. Chem.* **2018**, *57*, 7914−7924.

(50) Sugiki, S.-i.; Kurita, N.; Sengoku, Y.; Sekino, H. Fragment molecular orbital method with density functional theory and DIIS convergence acceleration. *Chem. Phys. Lett.* **2003**, *382*, 611−617.

(51) Sepehr, F.; Paddison, S. J. The solvation structure and thermodynamics of aqueous vanadium cations. *Chem. Phys. Lett.* **2013**, *585*, 53−58.

(52) Li, L.; Kim, S.; Wang, W.; Vijayakumar, M.; Nie, Z.; Chen, B.; Zhang, J.; Xia, G.; Hu, J.; Graff, G.; et al. A stable vanadium redox-flow battery with high energy density for large-scale energy storage. *Adv. Energy Mater.* **2011**, *1*, 394−400.

(53) Noack, J.; Roznyatovskaya, N.; Kunzendorf, J.; Skyllas-Kazacos, M.; Menictas, C.; Tübke, J. The influence of electrochemical treatment on electrode reactions for vanadium redox-flow batteries. *J. Energy Chem.* **2018**, *27*, 1341−1352.

(54) Wilkins, P. C.; Johnson, M. D.; Holder, A. A.; Crans, D. C. Reduction of vanadium (V) by L-ascorbic acid at low and neutral pH: kinetic, mechanistic, and spectroscopic characterization. *Inorg. Chem.* **2006**, *45*, 1471−1479.

(55) Steunou, N.; Livage, J. Rational design of one-dimensional vanadium (v) oxide nanocrystals: an insight into the physico-chemical parameters controlling the crystal structure, morphology and size of particles. *CrystEngComm* **2015**, *17*, 6780−6795.

(56) Timofeeva, M. N.; Panchenko, V. N.; Khan, N. A.; Hasan, Z.; Prosvirin, I. P.; Tsybulya, S. V.; Jhung, S. H. Isostructural metal-carboxylates MIL-100 (M) and MIL-53 (M)(M: V, Al, Fe and Cr) as catalysts for condensation of glycerol with acetone. *Appl. Catal., A* **2017**, *529*, 167−174.

(57) Sadeghi, O.; Amiri, M.; Reinheimer, E. W.; Nyman, M. The Role of Bi^{3+} in Promoting and Stabilizing Iron Oxo Clusters in Strong Acid. *Angew. Chem., Int. Ed.* **2018**, *57*, 6247−6250.

(58) Crans, D. C. Aqueous chemistry of labile oxovanadates: relevance to biological studies. *Comments Inorg. Chem.* **1994**, *16*, 1−33.

(59) Bussi, G.; Laio, A.; Parrinello, M. Equilibrium Free Energies from Nonequilibrium Metadynamics. *Phys. Rev. Lett.* **2006**, *96*, 090601.

(60) Towns, J.; Cockerill, T.; Dahan, M.; Foster, I.; Gaither, K.; Grimshaw, A.; Hazlewood, V.; Lathrop, S.; Lifka, D.; Peterson, G. D.; et al. XSEDE: Accelerating Scientific Discovery. *Comput. Sci. Eng.* **2014**, *16*, 62−74.